SCIENTIFIC PAPER

SOYBEAN OIL PYROLYSIS IN A CONTINUOUS BENCH-SCALE REACTOR FOR LIGHT OLEFIN PRODUCTION

Vinicyus Rodolfo Wiggers[1*], Robson Gil de Souza Ramos [1], Gabriel Henrique Wienhage [1], Tuanne Gomes Porto [1], António André Chivanga Barros [2], Luana Marcele Chiarello [1]

[1]*Department of Chemical Engineering, Regional University of Blumenau, Blumenau, SC, Brazil*

[2]*Instituto Superior Politecnico de Tecnologias e Ciencias, Luanda, Angola*

https://doi.org/10.2298/CICEQ240226033W

Received 26.2.2024.

Revised 20.9.2024.

Accepted 23.10.2024.

* Vinicyus R. Wiggers
E-mail: vwiggers@furb.br – Phone: +55 (47) 3221-6055

ABSTRACT

This study investigated the gas yield and its composition in different operation temperatures, giving special attention to light olefin production and oxygen content in soybean oil pyrolysis. The experiments were conducted in a continuous bench-scale reactor at steady state and isothermal conditions. Temperatures ranged from 500 to 600 °C with constant feeding mass flow. The resulting bio-oil exhibited high acid and iodine indices, as expected. Biogas samples were collected and submitted to gas chromatography to determine the chemical composition. The results revealed that ethene and propene formation are intensified with temperature, reaching more than 30% values in the gas phase. Additionally, higher temperatures led to increased oxygen removal from the triglyceride.
Keywords: Cracking, Ethene, Propene, Renewables, Triglycerides, Pyrolysis.

HIGHLIGHTS

- Study of temperature's impact on light olefin production in continuous soybean oil pyrolysis.
- The temperatures were varied from 500 to 600 °C in a constant feeding mass flow.
- Ethene and propene formation are intensified with temperature.
- The oxygen removal from the triglyceride also increases with temperature.

INTRODUCTION

In 2019, the global energy matrix primarily consisted of non-renewable sources such as coal, oil, and natural gas, accounting for over 84% of the energy matrix [1]. By 2021, renewable energy sources reached a total of approximately 6.7% [2].

The increasing energy demand, driven by a new phase of economic growth, particularly in developing nations, has outstripped available energy resources. Consequently, biomass emerges as a promising renewable energy option, primarily due to its abundant supply of agricultural, industrial, and household waste [3]. In the search of sustainable energy sources, biomasses that are edible are frequently considered. This fact can lead to a food versus energy competition. However, this practice aligns with circular economy principles by closing the loop between consumption and production, minimizing the environmental footprint. Additionally, waste biomass, used cooking oils and non-edible oils might create new markets for byproducts and reduce the dependence of petroleum advancing renewable sources goals without compromising food security [4].

Waste-to-energy technologies are frequently acknowledged as a viable solution for both energy production and waste management [5]. Notably, thermal conversion processes such as incineration [6], pyrolysis [7], and gasification [8] have gained prominence in this regard.

Thermal cracking, also known as pyrolysis, has emerged as one of the main potential processes to convert biomass into liquid fuels [9,10]. Thermal cracking involves the thermal degradation of biomass at high temperatures, ranging from 400 °C to 700 °C, in the absence of oxygen, with or without catalysts [11-13]. The pyrolysis of triacylglycerols involves breaking the carbon chains of animal or vegetable oils by increasing the system's temperature, resulting in solid, liquid, and gaseous phases [14]. The solid phase is basically coke with a high C/H ratio. By increasing the temperature, the reaction leads to the formation of low molecular weight organic products. These products are converted to CO_2, H_2, CO, CH_4, and C_2-C_4 hydrocarbons at high temperatures and increase gas production [15]. The organic liquid product, frequently called bio-oil, is composed mainly of hydrocarbons, which can be fractionated [16,17]. The yield and composition of the products obtained in the cracking process depend highly on the raw material [18] and operational conditions, especially the temperature-residence time combination. An elevated temperature with a long residence time will promote the formation of gaseous products, while a low temperature and a long residence time will favor coke formation. Finally, a moderate temperature with a short residence time will yield higher liquid product [19].

The ongoing global economic growth indicates a substantial rise in demand for raw materials in the chemical industry, thereby requiring a rise in the production of basic petrochemicals derived from petroleum naphtha, particularly ethene, and propene, which are the most widely used olefins in industrial applications [20]. They serve as building blocks for petrochemical chains, serving as precursors for plastics, fibers, elastomers, solvents, paints, adhesives, and various other products widely utilized by society today [21,22].

It is estimated that 400 million tons of olefins are produced annually, using one billion tons of hydrocarbons as raw materials through processes such as Fluid Catalytic Cracking (FCC), steam cracking, and dehydrogenation, among others [23]. Among the compounds in the olefin group, ethene is one of the most significant importance to the industry. It is an unsaturated hydrocarbon comprising two carbon atoms bonded by a double bond. Due to the double bond between its carbons, it is a highly reactive compound that can participate in distinct reactions, converted into other compounds through halogenation, hydration, oxidation, alkylation, oligomerization, and polymerization reactions. It is the most important olefin in the petrochemical chain, with its

leading derivatives including polyethylene, ethylene oxide, ethylene glycol, dichloroethane, ethylbenzene, and linear α-olefins, among others [2020].

Propene is an unsaturated hydrocarbon composed of three carbon atoms, with two of them bonded by a double bond. It can be obtained through various processes, mainly thermal cracking and FCC [24]. Propene is the second most important raw material in the petrochemical industry and serves as a building block for an entire production chain, generating various products such as polypropylene, acrylonitrile, propylene oxide, cumene, and acrylic acid, among others. It is primarily obtained from a non-renewable source, such as petrochemical naphtha [2525].

In the literature, there are many works regarding the pyrolysis of triglycerides [18,26–30], and most of them focus on bio-oil yield and characterization. The gas phase has not received much attention regarding chemical composition, especially in C_2-C_4 identification and quantification, generally being grouped in lumps [31–33]. The main objective of this study is to evaluate the influence of temperature on the yield and composition of the gaseous fraction produced in the thermal cracking of refined soybean oil. Soybean oil was chosen as an abundant source of triglycerides around the world. This study becomes relevant due to the addition of experimental data on producing light olefins through the pyrolysis of soybean oil.

MATERIAL AND METHODS

Thermal cracking experiments

For the execution of thermal cracking experiments, a bench-scale reactor was used, operating in a continuous regime under steady-state and isothermal conditions [34,35]. The stainless-steel auger reactor has a positive displacement pump responsible for constant and continuous feeding to the reactor (**Figure 1**). The reactor consists of a cylindrical tube with internal thread, built in stainless steel tubes measuring 955 mm in length and 25 mm in internal diameter, whose screw geometric dimensions can be seen in detail in [36]. The section comprises four control loops to maintain the reactor at a constant temperature. Each loop consists of 2 kW electric resistances. Before biomass feeding, water was passed through the reactor to produce steam and purge the oxygen. The feed contains only soybean oil, so during the processing only the feedstock is inside the reactor that works with pressure slightly above atmospheric pressure, avoiding the entrance of oxygen. After each experiment, water is passed again to purge remaining biogas, followed by high temperature air flow to burn the formed coke, as a reactor cleaning procedure.

Experimental runs were conducted at five different temperatures: 500, 525, 550, 575, and 600 °C, with a fixed mass flow rate of 300 g/h, in triplicate. The commercial refined soybean oil from the COAMO was obtained in 900 mL PET bottles from a local supplier and stored at room temperature (25°C).

Figure 1.

Soybean oil was fed to the thermal cracking reactor for one hour. Equation 1 was used to calculate the average reactor temperature for each experiment.

$$\bar{T}_{reactor} = \frac{\bar{T}_2+\bar{T}_3+\bar{T}_4+\bar{T}_5}{4} \quad (1)$$

where:

$\bar{T}_{reactor}$ is the average temperature of the reactor;

$\bar{T}_2$ is the average temperature registered at thermocouple 2;

$\bar{T}_3$ is the average temperature registered at thermocouple 3;

$\bar{T}_4$ is the average temperature registered at thermocouple 4;

$\bar{T}_5$ is the average temperature registered at thermocouple 5.

The volumetric flow of biogas generated during the reaction was measured to close the system's mass balance. A silicone hose connected to the reactor's outlet was inserted into a graduated inverted cylinder filled with water. The volumetric flow rate of the biogas was determined by measuring the time it took for the gas to displace the liquid in the cylinder. At least three samples of biogas were collected during the experiment using 60 mL syringes, which were connected to a 3-way valve and immediately taken for chromatographic analysis to determine the chemical composition. After each experiment, the mass of the produced bio-oil was measured, and physical-chemical analyses were carried out to characterize the obtained products.

Biogas composition

For the analysis of non-condensable gases, a Shimadzu® GC-17A gas chromatograph was used, equipped with a 60/80 Carboxen 1000 column (5 m x 2 mm stainless steel tubing). H_2, O_2, and N_2 were determined by thermal conductivity detection (TCD), while CH_4, C_2H_4, and C_2H_6 were detected using flame ionization detection (FID). CO and CO_2 were determined through methanation and FID, as described by Beims et al. [36].

For the analytical determination of C_3H_6, C_3H_8, C_4H_{10}, and C_4H_8, a gas chromatograph with FID detector, model 7890B from Agilent Technologies, was used, together with a capillary column, Stabilwax (30 m x 0.25 mm x 0.25 μm). The initial oven temperature was set at 28 °C (15 min) - 1 °C/min until 35 °C (2 min), followed by 30 °C/min until 100 °C (0 min), with a total run time of 32 min. The injector temperature was set at 250 °C, the helium gas flow rate at 2.2 mL/min, and the injection volume at 1 μL of the pure sample with a split ratio 100:1.

Bio-oil characterization

Bio-oil collected in the reservoirs was analyzed regarding specific gravity, acid and iodine indexes[37-39], and carbon number in the carbon chain. The methodology is described below.

Tests to determine the specific gravity were carried out in bio-oil samples produced in the reactor. The method is based on NBR-7148, being carried out at room temperature with the aid of a pycnometer, calibrated volumetric glassware, to determine the relationship sample mass/volume. The Acid Index (AI) is defined as the amount (in mg) of potassium hydroxide required to neutralize one gram of the sample. The AI test was conducted to compare the acid content present in each bio-oil produced. The test for determining the acid index test was carried out according to the standards established by ASTM D 974/2008. A 2g sample was placed in a 125 mL Erlenmeyer flask, and 25 mL of solvent (isopropanol) was added. Two drops of phenolphthalein indicator were then added to this mixture, followed by titration with a potassium hydroxide solution (0.1 mol/L) until a pink color appeared. The acid index was calculated using the Equation 2.

$$AI = (V_2 V_1) C_{KOH} 56{,}1/m \quad (2)$$

where, IA is the acid number (mg KOH/g sample), V2 is the volume spent in sample titration (ml), V1 is the volume spent on blank titration (ml) and m is the mass of the sample (g).

Following EN14111, the Iodine Index (II) was used for samples of the raw material and bio-oil obtained from the reaction. The II is directly related to the degree of unsaturation in the sample, with a higher iodine index indicating a greater number of double bonds (unsaturations) present in the oil.

The methodology consists of adding between 0.13 and 0.15 g of the sample to a 500 mL Erlenmeyer flask containing 20 mL of solvent solution (cyclohexane and glacial acetic acid, 1:1). Then, 25 mL of Wijs solution (commercial) is added, the flask is sealed, and the mixture is left in a dark environment for 1 hour. The same procedure is performed for the blank sample. After the reaction time is complete, 20 mL of KI (100 g/L) and 150 mL of distilled water are added. Titration is then carried out with sodium thiosulfate until the endpoint (from pale yellow to transparent). Next, 2 mL of starch solution is added, and the titration is continued until the solution becomes fully transparent. The II can then be calculated using Equation 3:

$$AI = 12.69N(V_2 V_1) \quad (3)$$

Where II is the iodine index of the sample (gI2/100g sample), N is the normality of the sodium thiosulfate, V1 is the volume of the blank (mL), V2 is the volume of the solution with the sample (mL), and m is the mass of the sample (g).The carbon number analysis was conducted on a Shimadzu® gas chromatograph (GC), model GC-2010 with AOC-5000 autoinjector and flame ionization detector (FID), the RTX-1 capillary column (30 m 0.32 mm x 3.00 μm) with helium gas flow of 1 mL/min. The initial heating of the oven was 50 ºC and remained for 5 min. Afterward, a rate of 5 ºC/min was applied up to 280 ºC, remaining at this temperature for 12 min. The injector temperature was 250 ºC, and the detector temperature was 280 ºC. The split was 1:100.

The identification of carboxylic acid and ester compounds was carried out using gas chromatography coupled to mass spectrometry (GC–MS) on Shimadzu GC–MS equipment (QP 2010 Plus) with a capillary column with RTX-5 with AOC-20i automatic injector. In addition to the NIST 08 Spectro library, standards of n-alkanes and fatty acid methyl esters (FAME) were injected to compare and identify compounds. The oven temperature was programmed to 50 ºC (2 min), heating at 5 ºC/min until 280 ºC (12 min). Helium was used as carrier gas with a constant 1 mL/min flow. The injector temperature was 250 °C, and the injection volume was 0.2 μL (pure sample) with a split ratio 1:200.

Mass balance of cracking products

The liquid and gas fraction yields were calculated according to equations already reported by Beims et al. [26,36]. The coke fraction is calculated by balance, the difference between the gas and liquid fractions. The coke on the reactor walls is removed during the cleaning process after each experimental run. The cleaning process involves feeding air into the heated reactor, promoting controlled burning. Equations 4, 5, 6, and 7 were used to calculate the fractions of bio-oil, biogas, and coke.

$$m_{SO} = m_{BO} + m_{BG} + m_{coke} \quad (4)$$

$$X_{BO} = \frac{m_{BO}}{m_{SO}} \quad (5)$$

$$X_{BG} = \frac{m_{BG}}{m_{SO}} \quad (6)$$

$$X_{coke} = 1 - X_{BO} - X_{BG} \quad (7)$$

where X_{BO}, X_{BG}, and X_{coke} are, respectively, the mass fractions of bio-oil, biogas, and coke, respectively.

RESULTS AND DISCUSSION

Pyrolysis experiments of refined soybean oil were carried out with material feed ($\dot{m}_{SO}$) varying between 301 and 315 g/h. The operating time was fixed in 1 hour and the temperature ($\bar{T}_{reactor}$) varied between 500 and 600 ºC. As the reaction temperature increased, there is a reduction in the yield of liquid fractions. This fact can be explained by the tendency of fragmentation of the initial molecule, leading to the formation of compounds with smaller molecular chains and, consequently, a higher gaseous fraction. Table 1 presents the actual resulting operational conditions, the mass yields of crude bio-oil ($\dot{m}_{BO}$) produced, and the volumetric flow of non-condensable gases ($\dot{V}_{BG}$) obtained during the experiments. It demonstrates that the conversion of soybean oil into non-condensable gases increases as the reaction temperature advances. At the same time, in the opposite direction, there is a reduction in the yield of the liquid fraction. The results showed that the highest amount of bio-oil produced (224 g/h) was obtained at T-500, while the highest flow of non-condensable gases (147.6 L/h) was achieved at T-600. On the other hand, the experiment carried out at T-600 showed a lower bio-oil yield (99.2 g/h) compared to the experiment at T-500. Likewise, the lowest flow of non-condensable gases (39.7 L/h) was recorded in the experiment at T-500.

Table 1.

Specifications**:** [1]Experiment run; [2]Average reactor temperature; [3]Soybean oil mass flow rate; [4]Bio-oil mass flow rate; [5]Biogas volumetric flow; [6]Average molecular mass of bio-oil; [7]Specific mass of biogas; [8]Biogas mass flow; [9]Composition of the biogas fraction; [10]Composition of the bio-oil fraction; [11]Coke fraction composition.

The results of the physicochemical analyses of bio-oil are shown in Table 2. The reaction temperature influenced the increase in the acidity index of the produced bio-oil, indicating the presence of fatty acids (saturated and unsaturated) and short-chain carboxylic acids in the final product. The high acidity can be explained by breaking C-C bonds rather than decarbonylation and decarboxylation reactions. The values for the iodine index represent the number of unsaturated compounds, indicating a high concentration of olefins, typical in cracking processes.

Table 2.

Figure 2 presents the compound distribution of bio-oils according to the carbon number in the chain. High temperatures lead to a higher concentration of lighter compounds, while lower temperatures result in a bio-oil with heavier ones. Figure 3 presents the GC-MS chromatograms for bio-oils obtained and the fatty acididentification. The peak intensity of identified fatty acids (palmitic, eicosanoic, stearic, oleic, and linoleic acids) reduces with temperature due to the advance of decarbonylation and decarboxylation reactions resulting in oxygen removal. The comparison with an n-alkanes standard sample shows that bio-oils have a wide range distribution of compounds according to the chain length. Furthermore, the acidity and the presence of olefins in high concentrations in the bio-oil produced indicates that it requires further treatment before being used as a source of fuels and chemicals.

Figure 2.

Figure 3.

Table 1 also shows the influence of the reaction temperature on the products' yield, showing a tendency towards a reduction in the production of bio-oil and an increase in the flow of non-condensable gases with the increase in temperature. During cracking experiments, gaseous samples collected were submitted to

chromatography to determine the molar and mass composition, presented in Table 2. With these data, the average molecular mass and density (ρ) of the bio-gas were determined and was possible to quantify mass yield of bio-gas and close the mass balance of the experiments, which data are also presented in Table 1. The average molecular weight decreases, and bio-gas yield increases with temperature. Also, it is possible to note that coke and gas have a significant yield at T-600. The presence of CO and CO_2 confirms the oxygen removal during pyrolysis. The hydrogen concentrations on a mass basis are not relevant. Ethene and propene concentrations are significant.

Table 3.

When analyzing the gaseous phase product, a significant variation in the concentrations of some components was observed with the increase in the reaction temperature. Methane (CH_4), ethene (C_2H_4), propene (C_3H_6), and hydrogen (H_2) increased in concentration with reaction temperature. Ethane (C_2H_6), carbon monoxide (CO), and carbon dioxide (CO_2) showed a reverse trend because of the increased concentration of light hydrocarbons resulting from more intensive cracking. As presented by Asikin-Mijan et al. [40], CO and CO_2 are formed by decarbonylation and decarboxylation reactions, respectively. The formation of CO and CO_2 results in the release of the radicals R and R', which undergo several subsequent reactions to form hydrocarbons in the C1-C5 range. The variation in the concentration of the mentioned components with the reaction temperature suggests that the high temperature favors the formation of large amounts of methane. On the other hand, the opposite trend exhibited by ethane indicates that hydrogen transfer reactions such as hydrogenation are more favorable at low temperatures. The elimination of hydrocarbon radicals and the dehydrogenation reactions for forming ethene from ethane or ethyl radicals may be favored at high temperatures. These results agree with the study performed by Idem et al. [41] and suggest that temperature is an important factor influencing the chemical reactions involved in the thermal cracking of soybean oil. With the molar composition of the bio-gas, it is possible to estimate its molecular weight and quantify its mass produced.

Table 4 brings the calculated mass flow of CO and CO_2, the calculated mass flow of oxygen, and its percentual removal according to the feeding mass flow of soybean oil. The mass flow of CO and CO_2 continues to increase with temperature as a result of deoxygenation reactions occurrence. However, the intensity of cracking also increases with temperature and leads to an improvement in light hydrocarbon formation resulting in decrease in the concentration of CO and CO_2 in the gas phase. It was also observed that the oxygen removal reactions continue to occur with temperature, reaching a value of ~10% at T-600. Since soybean oil has oxygen content varying in the range of 10-13% [42], pyrolysis can achieve high oxygen removal values at elevated temperatures.

Table 4.

CONCLUSIONS

The investigation shows that composition of gas phase must be carefully determined once overall mass balance depends on it. The analyses confirm that operational conditions, especially temperature, directly influence ethene and propene yields in the gas phase. At a temperature of 600 C, biogas production approaches nearly 50%, with more than 30% of ethene on a mass basis. Additionally, the oxygen removal in the form of CO and CO_2 increases with temperature, reaching high levels of oxygen removal.

ACKNOWLEDGMENTS The authors are grateful to the Regional University of Blumenau (FURB) and the Instituto Superior Politecnico de Tecnologias e Ciencias.

FUNDING

This work was supported by the Foundation for Research Support and Innovation of Santa Catarina State (FAPESC) and the Conselho Nacional de Desenvolvimento Científico e Tecnológico (CNPq no 302903/2023-2). This study was financed in part by the Coordenação de Aperfeiçoamento de Pessoal de Nível Superior e Brasil (CAPES) Finance Code 001.

COMPETING INTERESTS

The authors declare no competing interests.

REFERENCES

1. M. Heydari, A. Heydari, M. Amini, Int. J. Eng. Appl. Sci. 9 (2023) 167-173. https://ssrn.com/abstract=4515903
2. O.O. Yolcan, Innov. Green Dev. 2 (2023) 100070. https://doi.org/10.1016/j.igd.2023.100070
3. T. Li, J. Wang, H. Chen, W. Li, P. Pan, L. Wu, G. Xu, H. Chen, Energy Convers. Manage. 287 (2023) 117085. https://doi.org/10.1016/j.enconman.2023.117085
4. J. Tomei, R. Helliwell, Food versus fuel. Going beyond biofuels. Land Use Policy, 56 (2016). http://dx.doi.org/10.1016/j.landusepol.2015.11.015
5. T.C. Floriani, L.M. Chiarello, T.G. Porto, V.R. Wiggers, J. Solid Waste Technol. Manage. 48 (2022) 270–279. https://doi.org/10.5276/JSWTM/2022.270
6. B.E. Piske, F. Lopes, J. Utzig, V.R. Wiggers, Renewable Energy Power Qual. J. 21 (2023) 154–159. https://doi.org/10.24084/repqj21.255
7. L. Chiarello, T. Porto, A. Barros, E. Simionatto, V. Botton, V. Wiggers, Angolan Miner. Oil Gas J. 1 (2020) 1-5. https://doi.org/10.47444/amogj.v1i1.1
8. T.G. Porto, W.O. Tavares, F. Lopes, D. Vênancio, G.H. Wienhage, L.M. Chiarello, V.R. Wiggers, Angolan Miner. Oil Gas J. 2 (2021) 28-31. https://doi.org/10.47444/amogj.v2i2.5
9. Y. Shirazi, S. Viamajala, S. Varanasi, Appl. Energy 179 (2016) 755–764. https://doi.org/10.1016/j.apenergy.2016.07.025
10. D.G. Lima, V.C.D. Soares, E.B. Ribeiro, D.A. Carvalho, É.C.V. Cardoso, F.C. Rassi, K.C. Mundim, J.C. Rubim, P.A.Z. Suarez, J. Anal. Appl. Pyrolysis, 71, 987, 2004. https://doi.org/10.1016/j.jaap.2003.12.008.
11. L.M. Chiarello, T.G. Porto, G.H. Wienhage, V. Botton, V.R. Wiggers, in Handbook of Biomass Valorization for Industrial Applications, Shahid-ul-Islam, A.H. Shalla, S.A. Khan Eds., Wiley (2022) p. 107-128. https://doi.org/10.1002/9781119818816.ch6
12. S. Czernik, V Bridgwater, Energy Fuels 18 (2004) 590-598. https://doi.org/10.1021/ef034067u
13. G. Menshhein, V. Costa, L. M. Chiarello, D.R. Scharf, E.L. Simionato, V. Botton, H.F. Meier, V.R. Wiggers, L. Ender, Renewable Energy 142 (2019) 561-568. https://doi.org/10.1016/j.renene.2019.04.136
14. V.R. Wiggers, R.F. Beims, L. Ender, E.L. Simionatto, H.F. Meier, in Frontiers in Bioenergy and Biofuels, E. Jacob-Lopes, L.Q. Zepka Eds., InTech Open (2017) p. 524. http://doi.org/10.5772/65498
15. X. Hu, M. Gholizadeh, J. Energy Chem. 39 (2019) 109-143. https://doi.org/10.1016/j.jechem.2019.01.024
16. T. Stedile, R.F. Beims, L. Ender, D.R. Scharf, E.L. Simionato, H.F. Meier, V.R. Wiggers, Brazilian J. Chem. Eng. 36 (2019) 573-585. https://doi.org/10.1590/0104-6632.20190361s20170466
17. G. Menshhein, V. Costa, L.M. Chiarello, D.R. Scharf, E.L. Simionato, V. Botton, H.F. Meier, V.R. Wiggers, L. Ender, Data Brief 25 (2019) 104325. https://doi.org/10.1016/j.dib.2019.104325
18. T. Stedile, L. Ender, H.F. Meier, E.L. Simionatto, V.R. Wiggers, Renewable Sustainable Energy Rev. 50 (2015) 92-108. https://doi.org/10.1016/j.rser.2015.04.080
19. A. V. Bridgwater, Chem. Eng. J. 91 (2003) 87-102. https://doi.org/10.1016/S1385-8947(02)00142-0
20. L. Zhang, R. Gao, L. Wang, C. Zhang, K. Jun, S. K. Kim, T. Zhao, H. Wan, G. Guan, Chem. Eng. J. 471 (2023) 1-14. https://doi.org/10.1016/j.cej.2023.144611
21. M. Felischak, T. Wolff, L. Alvarado Perea, A. Seidel-Morgenstern, C. Hamel, Chem. Eng. Sci. 210 (2019) 1-9. https://doi.org/10.1016/j.ces.2019.115246

22. S. Wang, L. Zhang, P. Wang, X. Liu, Y. Chen, Z. Qin, M. Dong, J. Wang, L. He, U. Olsbye, W. Fan, Chem 8 (2022) 1376-1394. https://doi.org/10.1016/j.chempr.2022.01.004

23. V. Zacharopoulou, A. Lemonidou, Catalysts 8 (2017) 1-19. https://doi.org/10.3390/catal8010002

24. A. Payne, G. Garcia-Garcia, P. Styring, Green Chem. 25 (2023) 4029-4057. https://doi.org/10.1039/D2GC04721G

25. V. Zacharopoulou, A.A. Lemonidou, Mater. Today Proc. 5 (2018) 27511-27516. https://doi.org/10.1016/j.matpr.2018.09.070

26. R.F. Beims, V. Botton, L. Ender, D.R. Scharf, E.L. Simionato, H.F. Meier, W.R. Wiggers, Fuel 217 (2018) 175-184. https://doi.org/10.1016/j.fuel.2017.12.109

27. A. Goldbach, H. Meier, V. Wiggers, L. Chiarello, A. Barros, Chem. Ind. Chem. Eng. Q. 28 (2022) 1-8. https://doi.org/10.2298/CICEQ200810010G

28. M.A. Mohamed, Int. J. Res. Appl. Sci. Eng. Technol. (2017) 2971-2976. https://doi.org/10.22214/ijraset.2017.11410

29. E.S. Ramos, D. Zimmermann, R.F. Beims, L.M. Chiarello, V. Botton, E.L. Simionato, V.R. Wiggers, Environ. Prog. Sustainable Energy 39 (2020) 1-6. https://doi.org/10.1002/ep.13441

30. T. Kraiem, A.B. Hassen, H. Belayouni, M. Jeguirim, Sci. Pollut. Res., 24, 9951, 2017. https://doi.org/10.1007/s11356-016-7704-z.

31. B. Periyasamy, Fuel, 158, 479, 2015. https://doi.org/10.1016/j.fuel.2015.05.066.

32. C. Rabbat, S. Awad, A. Villot, Y. Andres, Waste Biomass Valorization 14 (2023) 2061-2083. https://doi.org/10.1007/s12649-022-01989-2

33. V. Botton, D.R. Scharf, E.L. Simionato, V.R. Wiggers, L. Ender, H.F. Meier, A.A. Chivanga Barros, Quim. Nova 35 (2012) 677-682. https://doi.org/10.1590/S0100-40422012000400004

34. M. Konig, L.M. Chiarello, L. Curbani, V. Botton, V.R. Wiggers, L. Ender, Ind. Crops Prod. 201 (2023) 1-7. https://doi.org/10.1016/j.indcrop.2023.116931

35. R.F. Beims, V. Botton, L. Ender, D.R. Scharf, E.L. Simionato, H.F. Meier, W.R. Wiggers, Data Brief 17 (2018) 442–451. https://doi.org/10.1016/j.dib.2018.01.054

36. M.J. Suota, E.L. Simionatto, D.R. Scharf, H.F. Meier, V.R. Wiggers, Energy Fuels 33 (2019) 9886–9894. https://doi.org/10.1021/acs.energyfuels.9b01971

37. G. H. Wienhage, E. S. Ramos, L. M. Chiarello, V. Botton, V. R. Wiggers, Angolan Miner. Oil Gas J. 2 (2021) 21-27. https://doi.org/10.47444/amogj.v2i2.4

38. A.S. Matheus, A.P.S. Francisco, P. Francisco, N. Manuela, A.A.C. Barros, Chem. Eng. Technol. 45 (2022) 1835-1841. https://doi.org/10.1002/ceat.202200171

39. N. Asikin-Mijan, H. V. Lee, J. C. Juan, A. R. Noorsaadahb, Y. H. Taufiq-Yap, RSC Advances. 7 (2017) 46445–46460. https://doi.org/10.1039/c7ra08061a.

40. R.O. Idem, S.P.R. Katikaneni, N.N. Bakhshi, Energy Fuels 10 (1996) 1150-1162. https://doi.org/10.1016/S0140-6701(97)82785-3

41. F. Yu, L. Gao, W. Wang, G. Zhang, J. Ji, J. Anal. Appl. Pyrolysis 104 (2013) 325-329. https://doi.org/10.1016/j.jaap.2013.06.017

FIGURE CAPTION

Figure 1. 3-D schematic view of the pyrolysis reactor.

Figure 2. Distribution of compounds in bio-oils according to carbon number.

Figure 3. GC–MS profiles for n-alkane standard and bio-oil samples at T-500, T-525, T-550, T-575 and T-600. Peaks: (a) palmitic acid, (b) eicosanoic acid, (c) stearic acid, (d) oleic acid and (e) linoleic acid.

Table 1. Experimental data on the thermal cracking of refined soybean oil.

Run[1]	$\overline{T}_{reactor}$[2] (ºC)	$\dot{m}_{SO}$[3] (g/h)	$\dot{m}_{BO}$[4] (g/h)	$\dot{V}_{BG}$[5] (L/h)	$\overline{MM}$[6] (g/mol)	ρ_{BG}[7] (g/L)	$\dot{m}_{BG}$[8] (g/h)	x_{BG}[9] (%)	x_{BO}[10] (%)	x_{coke}[11] (%)
T-500	$501.8^{\pm 6.7}$	$303.4^{\pm 1.6}$	$224.0^{\pm 7.0}$	$39.7^{\pm 3.6}$	$32.0^{\pm 2.1}$	$1.3^{\pm 0.1}$	$52.0^{\pm 5.8}$	$17.1^{\pm 1.8}$	$73.8^{\pm 2.6}$	$9.1^{\pm 2.3}$
T-525	$527.6^{\pm 3.7}$	$303.2^{\pm 0.9}$	$207.7^{\pm 7.5}$	$49.2^{\pm 5.7}$	$29.9^{\pm 0.9}$	$1.2^{\pm 0.0}$	$60.2^{\pm 7.9}$	$19.9^{\pm 2.7}$	$68.5^{\pm 2.6}$	$11.6^{\pm 4.8}$
T-550	$551.2^{\pm 3.1}$	$301.0^{\pm 0.8}$	$190.9^{\pm 9.1}$	$67.7^{\pm 3.8}$	$28.9^{\pm 0.3}$	$1.2^{\pm 0.0}$	$80.1^{\pm 5.3}$	$26.6^{\pm 1.7}$	$63.4^{\pm 3.1}$	$10.0^{\pm 1.4}$
T-575	$575.1^{\pm 1.8}$	$309.3^{\pm 4.5}$	$151.5^{\pm 9.8}$	$108.2^{\pm 6.2}$	$27.6^{\pm 1.5}$	$1.1^{\pm 0.1}$	$121.9^{\pm 1.2}$	$39.4^{\pm 0.3}$	$49.0^{\pm 3.7}$	$11.6^{\pm 4.0}$
T-600	$602.0^{\pm 2.5}$	$315.1^{\pm 3.2}$	$99.2^{\pm 18.8}$	$147.6^{\pm 4.4}$	$25.7^{\pm 1.0}$	$1.1^{\pm 0.0}$	$155.3^{\pm 10.4}$	$49.3^{\pm 2.8}$	$31.5^{\pm 5.6}$	$19.3^{\pm 8.4}$

[1] Experiment run
[2] Average reactor temperature
[3] Soybean oil mass flow rate
[4] Bio-oil mass flow rate
[5] Biogas volumetric flow
[6] Average molecular mass of bio-oil
[7] Specific mass of biogas
[8] Biogas mass flow
[9] Composition of the biogas fraction
[10] Composition of the bio-oil fraction
[11] Coke fraction composition

Table 2. Results of the physicochemical analyses of the acidity index (IA), iodine index (II), and specific mass (ρ_{BO}) of the crude bio-oil samples.

Run	IA (mg KOH/g)	II (g I_2/100 g)	$\rho_{BO}^{22^oC}$(kg/m³)
T-500	$101.9^{\pm 2.4}$	$184.9^{\pm 16.2}$	$895.4^{\pm 3.7}$
T-525	$120.8^{\pm 5.6}$	$213.2^{\pm 43.6}$	$896.3^{\pm 8.4}$
T-550	$127.5^{\pm 9.7}$	$249.7^{\pm 71.8}$	$894.8^{\pm 3.7}$
T-575	$123.6^{\pm 8.9}$	$341.1^{\pm 3.6}$	$891.6^{\pm 3.9}$
T-600	$120.9^{\pm 5.5}$	$310.3^{\pm 30.6}$	$902.2^{\pm 8.9}$

Table 3. Molar (m) and mass (w) composition of non-condensable gases (%).

Run	CO	CH_4	CO_2	C_2H_4	C_2H_6	C_3H_6	H_2	Others*
	(m/w)	(m/w)	(m/w)	(m/w)	(m/w)	(m/w)	(m/w)	
T-500	$25.5^{\pm5.7}/22.5^{\pm5.9}$	$9.0^{\pm2.2}/4.6^{\pm1.4}$	$14.2^{\pm1.0}/19.7^{\pm2.1}$	$22.9^{\pm2.0}/20.2^{\pm2.9}$	$11.1^{\pm0.7}/10.5^{\pm1.3}$	$6.6^{\pm6.2}/8.9^{\pm8.3}$	$2.4^{\pm0.4}/0.1^{\pm0.1}$	$8.2^{\pm10.5}/12.8^{\pm15.7}$
T-525	$23.1^{\pm1.1}/21.7^{\pm1.6}$	$12.0^{\pm0.9}/6.4^{\pm0.7}$	$10.7^{\pm0.1}/15.8^{\pm0.6}$	$29.3^{\pm1.0}/27.5^{\pm1.6}$	$12.8^{\pm0.7}/12.9^{\pm0.5}$	$6.9^{\pm1.8}/9.7^{\pm2.6}$	$1.8^{\pm0.4}/0.1^{\pm0.0}$	$3.4^{\pm3.8}/5.9^{\pm6.2}$
T-550	$20.6^{\pm1.7}/19.9^{\pm1.8}$	$14.5^{\pm0.4}/8.0^{\pm0.2}$	$9.1^{\pm0.5}/12.6^{\pm1.5}$	$31.8^{\pm0.4}/30.9^{\pm0.4}$	$12.9^{\pm0.5}/13.4^{\pm0.6}$	$7.9^{\pm1.1}/11.5^{\pm1.6}$	$2.0^{\pm0.2}/0.1^{\pm0.0}$	$1.3^{\pm1.4}/1.7^{\pm1.6}$
T-575	$20.5^{\pm0.4}/20.8^{\pm0.8}$	$15.4^{\pm1.0}/8.9^{\pm0.2}$	$8.3^{\pm0.1}/13.3^{\pm0.8}$	$31.7^{\pm1.9}/32.2^{\pm0.4}$	$9.5^{\pm0.7}/10.3^{\pm0.3}$	$8.7^{\pm1.6}/13.1^{\pm1.8}$	$5.5^{\pm5.5}/0.4^{\pm0.4}$	$0.5^{\pm0.1}/0.9^{\pm0.3}$
T-600	$18.4^{\pm1.2}/20.1^{\pm2.0}$	$15.4^{\pm1.1}/9.6^{\pm0.4}$	$7.5^{\pm0.4}/12.8^{\pm1.1}$	$29.7^{\pm1.9}/32.4^{\pm1.0}$	$8.6^{\pm0.6}/10.1^{\pm0.5}$	$8.2^{\pm1.9}/13.4^{\pm2.7}$	$11.9^{\pm3.5}/0.9^{\pm0.3}$	$0.4^{\pm0.1}/0.8^{\pm0.2}$

* C_3H_8, C_4H_8 and C_4H_{10} were not detected in biogas at different temperatures.

Table 4. Mass flow of CO ($\dot{m}_{CO}$), CO_2 ($\dot{m}_{CO_2}$), calculated mass flow of oxygen in biogas ($\dot{m}_{O-BG}$) and its percentual ratio related to the feeding mass flow ($\dot{m}_{SO}$).

Run	$\dot{m}_{CO}$ **(g/h)**	$\dot{m}_{CO_2}$ **(g/h)**	$\dot{m}_{O-BG}$ **(g/h)**	$\dot{m}_{SO}$ **(g/h)**	$\frac{\dot{m}_{O-BG}}{\dot{m}_{SO}}$ **(%)**
T-500	$11.3^{\pm 1.1}$	$10.4^{\pm 0.3}$	$14{,}0^{\pm 0{,}9}$	$303.4^{\pm 1.6}$	4,6
T-525	$13.0^{\pm 1.7}$	$9.5^{\pm 1.0}$	$14{,}3^{\pm 1{,}7}$	$303.2^{\pm 0.9}$	4,7
T-550	$15.9^{\pm 0.4}$	$11.1^{\pm 1.2}$	$17{,}1^{\pm 1{,}1}$	$301.0^{\pm 0.8}$	5,7
T-575	$25.3^{\pm 0.9}$	$16.2^{\pm 1.0}$	$26{,}3^{\pm 1{,}3}$	$309.3^{\pm 4.5}$	8,4
T-600	$31.1^{\pm 1.1}$	$19.8^{\pm 0.7}$	$32{,}2^{\pm 1{,}2}$	$315.1^{\pm 3.2}$	10,2

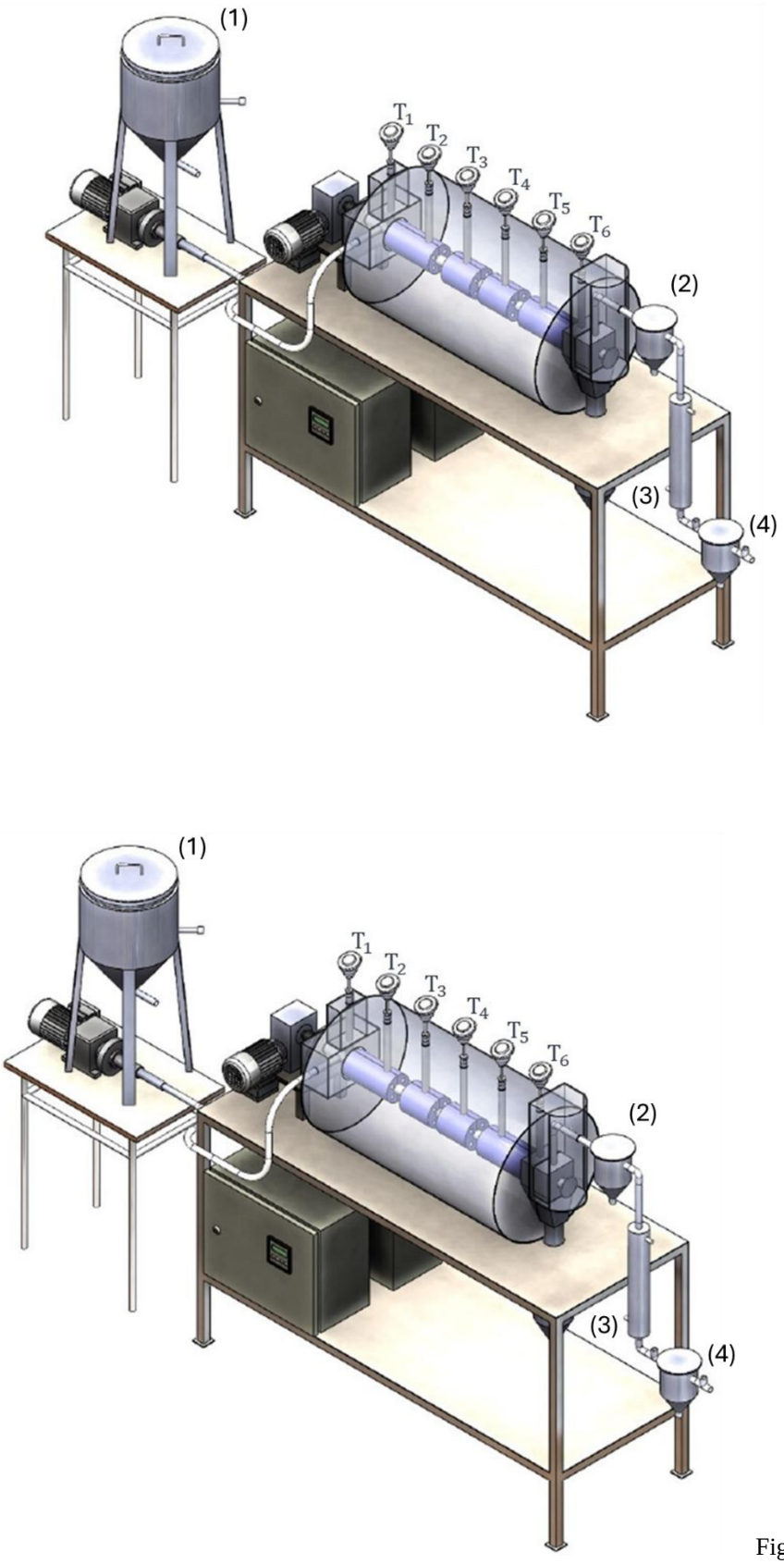

Figure 1

Note: (1) – Feedstock reservoir; (2) - First bio-oil reservoir; (3) – Condenser; (4) – Second bio-oil reservoir.

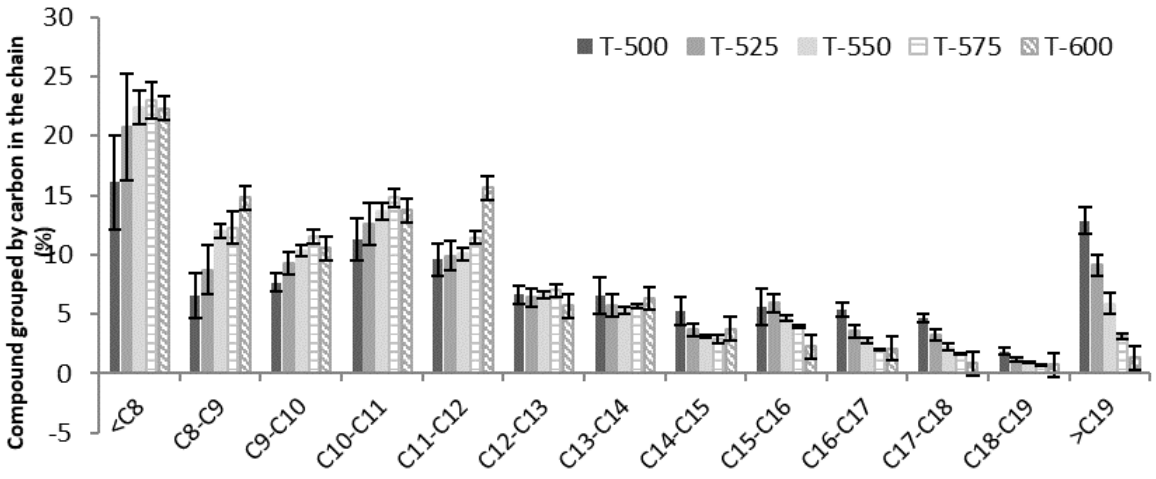
T-500
T-525
T-550
T-575
T-600
Compound grouped by carbon in the chain (%)
30
25
20
15
10
5
0
-5
<C8
C8-C9
C9-C10
C10-C11
C11-C12
C12-C13
C13-C14
C14-C15
C15-C16
C16-C17
C17-C18
C18-C19
>C19

Figure 2

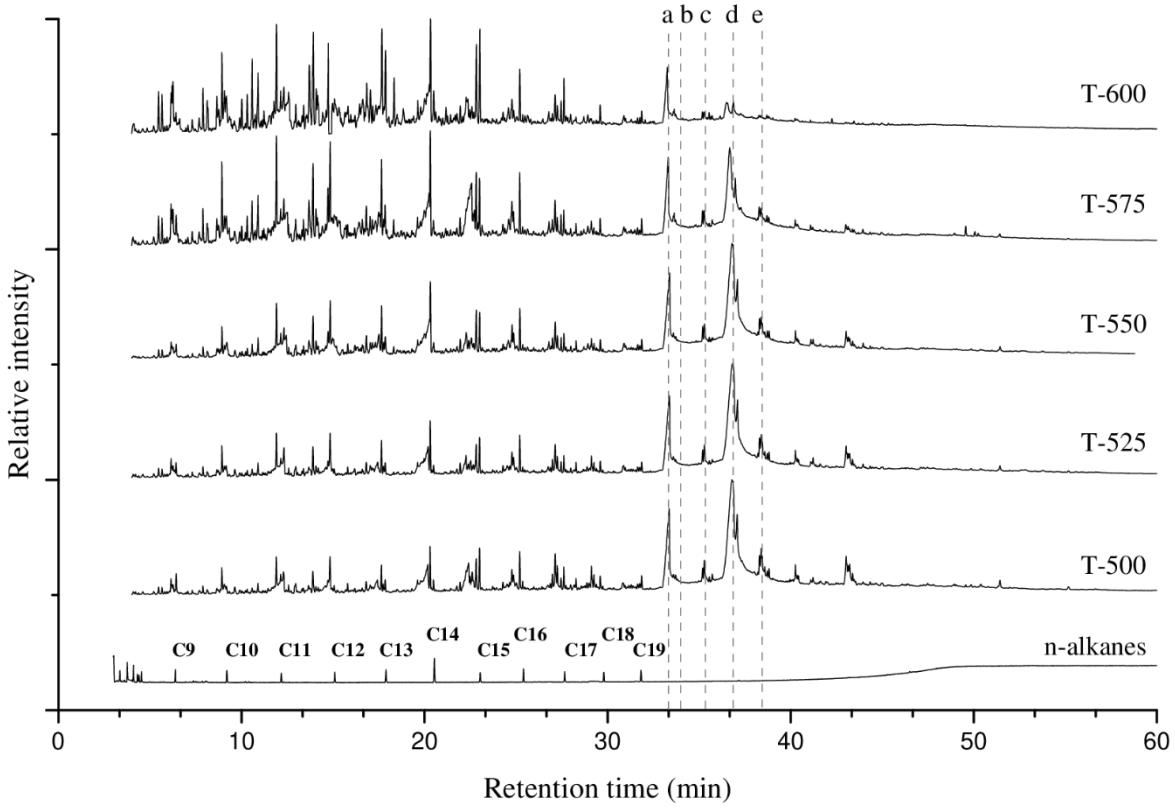
a b c d e
T-600
T-575
T-550
T-525
T-500
C9 C10 C11 C12 C13 C14 C15 C16 C17 C18 C19
n-alkanes
Relative intensity
0 10 20 30 40 50 60
Retention time (min)

Figure 3